Technique Report | Received 20 December 2022; Accepted 15 February 2023; Published 29 March 2023
https://doi.org/10.55092/bm20230002

Retarded release of small-molecule drugs from phase-separated dextran hydrogels through host-guest complexation

Ki Hyun Bae[1], Shengyong Ng[1], Li Li[1] and Motoichi Kurisawa[1,2,*]

[1] Institute of Bioengineering and Bioimaging (IBB), Agency for Science, Technology and Research (A*STAR), Singapore
[2] School of Materials Science, Japan Advanced Institute of Science and Technology, Nomi, Japan

* Corresponding author; E-mail: kurisawa@jaist.ac.jp.

Abstract: Hydrogels have emerged as promising materials for diverse applications in biomedicine and biotechnology, but their use as a drug carrier has been limited by the difficulty of achieving controlled drug release. Herein we report the development of phase-separated dextran hydrogels with 4-arm poly(ethylene glycol)-*β*-cyclodextrin (4-arm PEG-*β*CD) microdomains for prolonged release of small-molecule drugs. These hydrogels are designed to enhance the partition of drug molecules in the PEG microdomains through host-guest complexation, leading to delayed drug diffusion through the dextran gel matrix. Three different drugs (*β*-lapachone, imiquimod and oxaliplatin) were used to investigate the effect of 4-arm PEG-*β*CD on their partitioning behavior. The mechanical property and microdomain structure of the hydrogels were characterized by oscillatory rheology measurements and confocal laser scanning microscopy, respectively. Interestingly, we observed non-Fickian diffusion phenomena of *β*-lapachone and imiquimod from the phase-separated hydrogels, suggesting the potential applicability of host-guest interactions for the design of sustained drug release systems.

Keywords: phase separation; dextran; hydrogel; host-guest complexation; drug release

1. Introduction

Hydrogels represent a three-dimensional network of crosslinked water-soluble polymers which can hold a substantial volume of biological fluids [1]. Over the last few decades, hydrogels have attracted growing interest for a wide range of biotechnological applications, including drug delivery, regenerative medicine and wound repair because of their biologically relevant characteristics [2–4]. First, the soft surface and tissue-like elasticity of hydrogels can reduce mechanical stress to the surrounding tissue upon administration, thus providing great biocompatibility [5,6]. Second, the high water content (>95 wt%) of

hydrogels generates a low interfacial tension, which helps avoid serum protein adsorption and unwanted inflammatory response [7,8]. Lastly, the sponge-like porous network of hydrogels renders them with the ability to carry a relatively large quantity of drug payloads in their interior [9]. In spite of such beneficial properties, the application of hydrogels as drug carriers has been largely limited by the difficulty in regulating the drug release kinetics. For example, most hydrogel systems have a high permeability to small-molecule drugs and thus suffer from a 'initial burst effect', whereby a substantial fraction of the drug payload is liberated by simple diffusion during an initial time period [10]. This burst release can cause suboptimal drug usage and undesirable side effects associated with a rapid rise in blood drug levels following in vivo administration [11,12]. Hence, it is highly desirable to explore new types of hydrogels that can achieve better controlled drug release.

Aqueous two-phase polymer system (ATPS), an aqueous polymeric mixture that can separate into two immiscible phases, have been widely exploited for the liquid-liquid extraction and enrichment of diverse biomolecules and chemical compounds on the basis of their selective distribution in one of the two phases [13,14]. The most well-studied ATPS involves the combination of poly(ethylene glycol) (PEG) and dextran, which forms a PEG-rich top and dextran-rich bottom phase when mixed above certain concentrations [15]. By taking an advantage of the selective drug-partitioning property of ATPS, we have previously developed a phase-separated dextran-tyramine (Dex-Tyr) hydrogel containing micron-scale PEG domains as a drug reservoir for long-term sustained release of PEGylated protein drugs [16]. Although the phase-separated hydrogel effectively decreased the initial burst release of PEGylated proteins through their preferential partitioning in the PEG microdomains, this approach was not broadly applicable to non-PEGylated proteins and small-molecule drugs [17]. Recently, Kazuhiro *et al.* proposed a new approach to modulate the partitioning behavior of proteins in the PEG-dextran ATPS by exploiting the host-guest complexation [18]. The addition of *β*-cyclodextrin (*β*CD)-modified PEG was found to increase the distribution of adamantane-modified proteins in PEG-rich phase via the formation of an inclusion complex between *β*CD and adamantine group.

Motivated by the aforementioned finding, we herein aim to design phase-separated dextran hydrogels having 4-arm PEG-*β*CD microdomains for prolonged release of small-molecule drugs (Figure 1). Dextran, a homopolysaccharide composed of anhydroglucose, was chosen as a hydrogel-forming material due to its biodegradable and biocompatible nature [19]. The hydrogels were produced by adding diluted H_2O_2 and horseradish peroxidase (HRP) into a single-phase mixture of Dex-Tyr conjugate, 4-arm PEG-*β*CD and drug of interest. HRP-catalyzed crosslinking of Dex-Tyr conjugates initiated a phase separation and led to the spontaneous generation of 4-arm PEG-*β*CD domains dispersed within a continuous Dex-Tyr hydrogel matrix [20]. We hypothesized that the host-guest complexation between a drug and 4-arm PEG-*β*CD would delay the diffusional release of drug molecules by driving their partition into the discrete PEG microdomains. To test this hypothesis, the partition coefficients of three different drugs (*β*-lapachone, imiquimod and oxaliplatin) were evaluated

in ATPS composed of dextran/4-arm PEG or dextran/4-arm PEG-*β*CD. Moreover, we compared the drug release kinetics of Dex-Tyr, Dex-Tyr/4-arm PEG and Dex-Tyr/4-arm PEG-*β*CD hydrogels with identical storage moduli. Interestingly, the release of *β*-lapachone and imiquimod from Dex-Tyr/4-arm PEG-*β*CD hydrogels was governed by anomalous non-Fickian diffusion. Our proof-of-concept study demonstrated the feasibility of host-guest complexation to regulate the diffusional transport of small-molecule drugs from hydrogels.

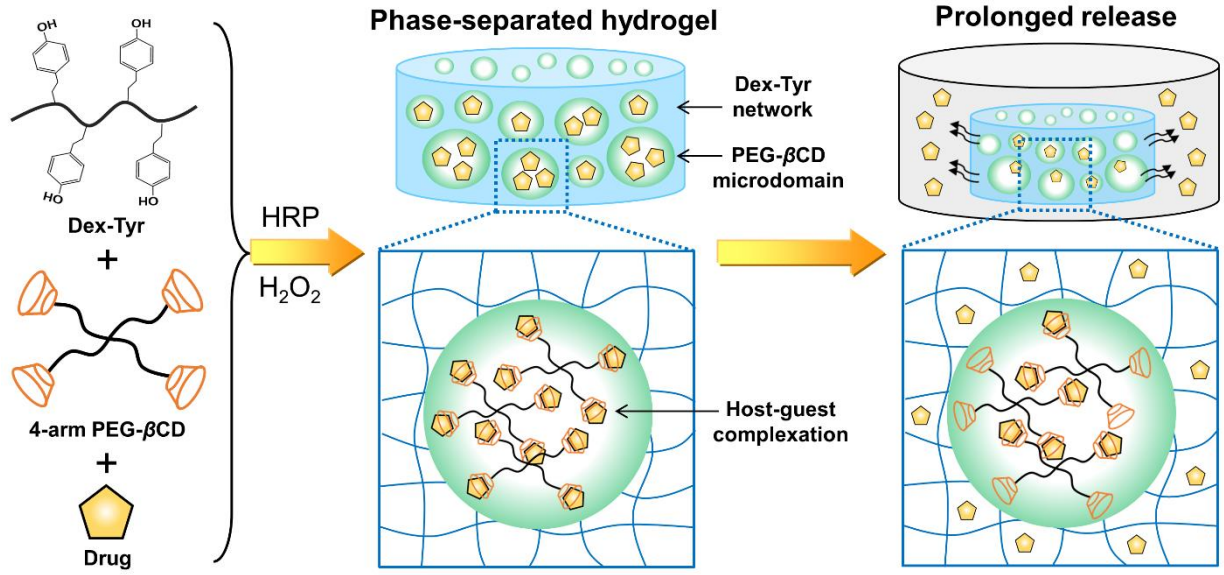

Figure 1. Scheme for the formation of a phase-separated dextran/4-arm PEG-*β*CD hydrogel and its application for prolonged drug release through host-guest complexation.

2. Methods

2.1. Materials

Dextran with average molecular weight (M_w) of 500 kDa, dextran-fluorescein isothiocyanate conjugate (FITC-dextran, M_w = 500 kDa), tyramine, ammonium acetate, oxaliplatin and 6-monodeoxy-6-monoamino-*β*-cyclodextrin hydrochloride (*β*CD-NH_2) were products of Sigma-Aldrich (Minnesota, USA). Star-shaped 4-arm PEG (M_w = 10 kDa) and 4-arm PEG-succinimidyl glutarate (4-arm PEG-SG, M_w = 10 kDa) were purchased from JenKem (Plano, USA). PEG-sulforhodamine (M_w = 10 kDa) was a product of Creative PEGWorks (Winston-Salem, USA). *β*-lapachone was purchased from Abcam (Cambridge, UK). Imiquimod was purchased from InvivoGen (San Diego, USA). HRP was obtained from Wako (Osaka, Japan). H_2O_2 was purchased from Lancaster Synthesis (Lancashire, UK). Deuterated dimethyl sulfoxide (DMSO-d_6) was obtained from Cambridge Isotope (Tewksbury, USA).

2.2. Synthesis of 4-arm PEG-βCD conjugate

To synthesize 4-arm PEG-*β*CD conjugate, 900 mg (0.09 mmol) of 4-arm PEG-SG was first placed in a 100-mL round-bottom flask. Then, 506 mg (0.432 mmol) of *β*CD-NH_2 was dissolved in 30 mL of 10 mM sodium phosphate buffer (pH 8) and added into the flask with continuous stirring. After stirring for 24 h at 37 °C, the mixture was moved to dialysis tubes with a M_w cutoff of 2 kDa. The tubes were subjected to dialysis against 10 mM ammonium acetate buffer (pH 7) for 3 d at 4 °C and deionized water for 2 d at 4 °C. The dialysis buffer was changed three times daily. The resultant solution was lyophilized to obtain 4-arm PEG-*β*CD conjugate (yield: 86.4%). ^{1}H NMR (400 MHz, DMSO-d_6, ppm): 5.65-5.85 (m, 14 H, OH-2,3), 4.83 (d, 7 H, H-1), 4.47 (d, 6 H, OH-6), 4.12 (t, 8 H, -(C=O)OCH_2-), 3.42-3.75 (m, 28 H, H-3,5,6 overlaps with PEG), 3.42-3.15 (m, H-2,4 overlaps with HOD), 2.31 (t, 8 H, -C(=O)CH_2-), 2.15 (t, 8 H, -NHC(=O)CH_2-), 1.72 (q, 8 H, -C(=O)CH_2CH_2-). The degree of modification (the number of *β*CD per conjugate) was estimated by an equation:

$$Degree\ of\ modification = \frac{A_{CD}/N_1}{\{(A_{PEG}-(A_{CD}/N_1\times N_2)\}/N_{PEG}} \quad (1)$$

where A_{CD} is the peak area of anomeric H-1 proton of *β*CD at 4.83 ppm, A_{PEG} is the peak area of the PEG backbone at 3.42-3.15 ppm, N_1 is the number of anomeric H-1 protons of *β*CD (total 7 protons), N_2 is the number of glucosidic protons of *β*CD (total 28 protons), and N_{PEG} is the number of PEG backbone protons (total 908 protons).

2.3. Determination of partition coefficients in aqueous two-phase solution

Dextran and 4-arm PEG-*β*CD conjugate were separately solubilized in phosphate-buffered saline (PBS, 10 mM, pH 7.4) at a concentration of 20 and 40% (w/v), respectively. To examine partition coefficients, 240 µL of dextran solution, 30 µL of 4-arm PEG-*β*CD solution, 30 µL of each drug solution were mixed in 1.5-mL microcentrifuge tubes. For comparison, ATPS composed of dextran and 4-arm PEG was also prepared using 30 µL of 4-arm PEG solution instead of 4-arm PEG-*β*CD solution. Tested drug solutions are listed as follows: *β*-lapachone (5 mM in 50% ethanol), imiquimod (3.6 mM in deionized water) and oxaliplatin (5 mM in deionized water). The mixture was left to phase-separate at 4 ºC for 1 h. The resulting PEG-rich top and dextran-rich bottom phases were carefully separated.

The concentration of *β*-lapachone and imiquimod in each phase was assessed by comparing their absorbance at 257 nm and 318 nm, respectively, with those of a series of standard solutions ([*β*-lapachone] = 0.3-20 µg mL^{-1}, [imiquimod] = 0.8–28 µg mL^{-1}). All UV-vis measurements were conducted in triplicates on a Hitachi U-2810 spectrophotometer (Hitachi, Japan). The concentration of oxaliplatin in each phase was determined by inductively coupled plasma (ICP) mass spectrometry according to a previously described method with some modification [21]. Briefly, 50 µL of sample solution was decomposed in 4.95 mL of 2% (v/v) nitric acid for 2 h at 25 ºC, and the platinum content was measured by comparing its ^{195}Pt signal intensity with those of a series of standard solutions ([Pt] = 0-100 ng mL^{-1}). All ICP-MS measurements were conducted in triplicates on an Elan DRC II mass

spectrometer (PerkinElmer, USA). The partition coefficient of a tested drug was calculated by dividing its concentrations in the top phase with those in the bottom phase.

2.4. Formation of Dex-Tyr/4-arm PEG-βCD hydrogels

Dex-Tyr conjugate was synthesized by activating the hydroxyl group of dextran with *p*-nitrophenyl formate and subsequently reacting it with the primary amine group of tyramine, as reported previously [16]. The degree of modification was estimated as 34 tyramine per conjugate by comparing the relative peak area of the aromatic protons of a tyramine moiety with those of anomeric H-1 proton of dextran in ^{1}H NMR spectrum (Figure S1). Dex-Tyr conjugate was first solubilized in PBS at a concentration of 20% (w/v). Separately, 4-arm PEG-*β*CD conjugate was prepared in PBS at a concentration of 40% (w/v). To produce Dex-Tyr/4-arm PEG-*β*CD hydrogels, 240 µL of Dex-Tyr solution, 30 µL of 4-arm PEG-*β*CD solution, 20 µL of PBS and 5 µL of HRP solution were mixed in a 1.5-mL Protein LoBind tube (Eppendorf, Germany). After 5 µL of H_2O_2 solution was added, the mixture was vortexed to obtain homogeneous solution. Subsequently, 210 µL of the solution was transferred to a HAAKE Rheoscope 1 (Karlsruhe, Germany) and then examined in the oscillatory mode with a constant frequency of 1 Hz at 37 ºC. The typical final concentration of HRP and H_2O_2 was 0.13 units mL^{-1} and 5.38 mM, respectively. The time-course change of storage modulus (G') and loss modulus (G'') was monitored. The gel point when reaching $G' = G''$ was examined as an indicator of gelation time. As a comparison group, Dex-Tyr/4-arm PEG hydrogels were produced using 30 µL of 4-arm PEG solution instead of 4-arm PEG-*β*CD solution. In this study, 0.13 units mL^{-1} HRP and 6.65 mM H_2O_2 were used to produce Dex-Tyr/4-arm PEG hydrogels having storage modulus identical to Dex-Tyr/4-arm PEG-*β*CD hydrogels. Dex-Tyr hydrogels with the same storage modulus were also prepared using 0.13 units mL^{-1} HRP and 5.38 mM H_2O_2. The dynamic strain sweep test was carried out using a 40-mm parallel plate under a constant angular frequency at 10 rad/s, whereas the dynamic frequency sweep test was conducted under a constant strain at 1%.

2.5. Observation of microdomain structure of Dex-Tyr/4-arm PEG-βCD hydrogels

FITC-dextran and PEG-sulforhodamine were separately solubilized in PBS at a concentration of 20% and 40% (w/v), respectively. Typically, 235 µL of 20% (w/v) Dex-Tyr solution, 5 µL of FITC-dextran solution, 25 µL of 40% (w/v) 4-arm PEG-*β*CD solution, 5 µL of PEG-sulforhodamine solution, 20 µL of PBS and 5 µL of HRP solution were mixed in a 1.5-mL Protein LoBind tube. After 5 µL of H_2O_2 solution was added, the mixture was vortexed to obtain homogeneous solution. Subsequently, 60 µL of the solution was transferred into a glass-bottomed microwell dish (MatTek, USA) and then sealed with a cover glass. The final concentration of HRP and H_2O_2 was 0.13 units mL^{-1} and 5.38 mM, respectively. The microwell dishes were then incubated at 37 °C for 1 h. The resultant hydrogels were imaged under a Zeiss LSM 5 DUO confocal microscope (Carl Zeiss, Germany).

2.6. Examination of drug release from Dex-Tyr/4-arm PEG-βCD hydrogels

To produce drug-loaded Dex-Tyr/4-arm PEG-*β*CD hydrogels, 240 µL of 20% Dex-Tyr solution, 30 µL of 40% 4-arm PEG-*β*CD solution, 20 µL of each drug solution and 5 µL of HRP solution were mixed in a 1.5-mL Protein LoBind tube. After 5 µL of H_2O_2 solution was added, the mixture was vortexed to obtain homogeneous solution. Subsequently, 210 µL of the solution was applied to the bottom of a 5-mL Protein LoBind tube. Tested drug solutions are listed as follows: *β*-lapachone (5 mM in 50% ethanol), imiquimod (3.6 mM in deionized water) and oxaliplatin (5 mM in deionized water). The final concentration of HRP and H_2O_2 was 0.13 units mL^{-1} and 5.38 mM, respectively. The tubes were incubated at 37 °C for 1 h. The produced hydrogel was immersed in 2.5 mL of PBS and then incubated at 37 ºC with a continuous shaking. For comparison, drug-loaded Dex-Tyr/4-arm PEG and Dex-Tyr hydrogels were also produced as described above. At designated time points, 0.2 mL of the release fraction was collected. The same volume (0.2 mL) of fresh PBS was replenished to the tube each time. The concentration of *β*-lapachone, imiquimod and oxaliplatin was quantified as described in the section 2.3. To assess drug release kinetics, the initial 60% of drug release data were fitted to the Ritger-Peppas equation:

$$\frac{M^t}{M^\infty} = kt^n \qquad (2)$$

where n is the diffusional exponent, k is a proportionality constant, and M^t and M^∞ are the quantity of drug liberated at time t and at equilibrium, respectively [22]. The cumulative drug release was determined by dividing the quantity of liberated drugs with the total quantity of drugs loaded in each hydrogel. To examine the integrity of *β*-lapachone released from Dex-Tyr/4-arm PEG-*β*CD hydrogels, the release medium taken at 192 h was put into a quartz cuvette and its fluorescence emission spectrum was obtained on the Cary Eclipse spectrometer (Agilent, USA) at an excitation wavelength of 320 nm with the use of excitation and emission slits of 5 and 5 nm, respectively.

2.7. Evaluation of the physiological stability of Dex-Tyr/4-arm PEG-βCD hydrogels

A pre-gel solution for Dex-Tyr/4-arm PEG-*β*CD hydrogels was prepared as described above and 210 µL of which were injected between two parallel glass plates clamped together with 1.5 mm spacing. Gelation was allowed to proceed for 2 h at 37 °C under a humid condition. The resultant hydrogel disk (12 mm diameter × 1.5 mm thick) was weighed to measure the initial gel weight (W_0). The hydrogel disks were placed in Accuvette II disposable containers (Beckman Coulter, USA) and then incubated in 5 mL of PBS (pH 7.4) at 37 °C with continuous shaking at 50 rpm. At predetermined time intervals, the buffer solution was removed from the container and the weight of the hydrogel disk (W_t) was recorded. Normalized gel weight (W_t/W_0) was calculated to assess the physiological stability of the hydrogels.

2.8. Statistical assessment

All obtained data were expressed as mean ± standard deviation (SD). Statistical assessment was performed using the GraphPad Prism 9 Software (GraphPad Software, USA). A calculated probability (*p*-value) smaller than 0.05 was considered to be significant statistically.

3. Results and Discussion

3.1. Synthesis of 4-arm PEG-βCD conjugate

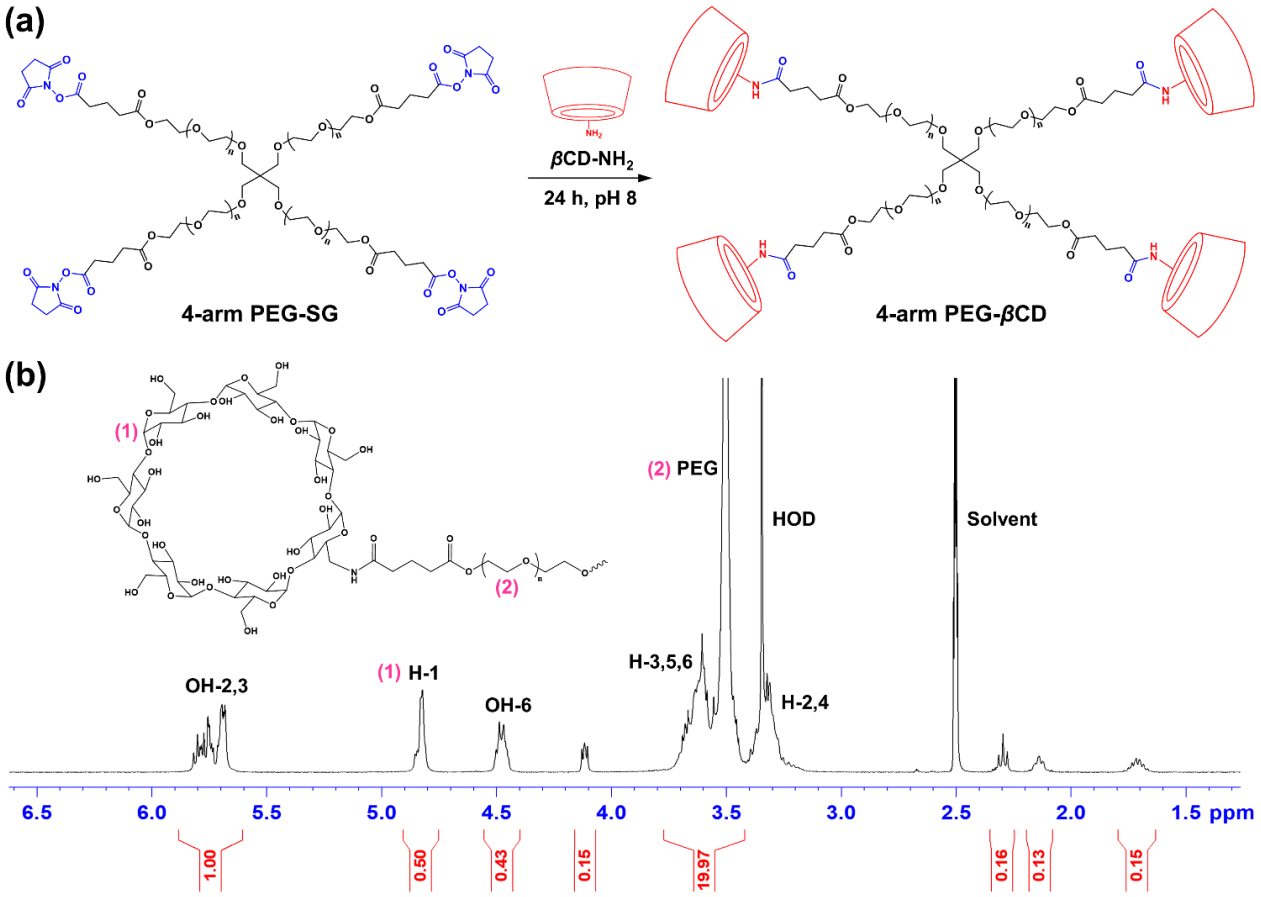

Figure 2. (a) Scheme for the synthesis of 4-arm PEG-*β*CD conjugate. (b) ^{1}H NMR spectrum of 4-arm PEG-*β*CD conjugate dissolved in DMSO-*d*6.

The star-shaped 4-arm PEG-*β*CD conjugate (M_w = 10 kDa) was synthesized through conjugation of the primary amine group of *β*CD-NH_2 to the succinimidyl ester group of 4-arm PEG-SG (Figure 2a). After reaction for 24 h at pH 8, the mixture was dialyzed for total 5 days at 4 °C with a M_w cutoff of 2 kDa to remove unreacted *β*CD-NH_2 and then lyophilized. The chemical structure of 4-arm PEG-*β*CD conjugate was examined by ^{1}H NMR spectroscopy. As shown in Figure 2b, the produced conjugate displayed characteristic proton signals of *β*CD (OH-2,3 at 5.65-5.85 ppm, H-1 at 4.83 ppm and OH-6 at 4.47 ppm) [23]

together with those of PEG backbone (methylene protons at 3.5 ppm) [24]. The degree of modification was estimated as 3.6 *β*CD per conjugate by comparing the relative peak area of the PEG backbone with those of anomeric H-1 proton of *β*CD.

3.2. Impact of 4-arm PEG-βCD on the partition coefficient of small-molecule drugs

We investigated the impact of 4-arm PEG-*β*CD on the partition coefficients of three different drugs: *β*-lapachone, imiquimod and oxaliplatin (Figure 3a). *β*-lapachone is a natural *ortho*-naphthoquinone compound that can stimulate the recovery of burn-wounded skin [25]. Imiquimod is a guanine nucleoside analog with potent antiviral activity [26], whereas oxaliplatin is a platinum-based DNA-alkylating agent that activates immunogenic cell death for cancer immunotherapy [27]. These drugs were selected for our study because they don't have phenol groups, which can interfere with HRP-catalyzed crosslinking reaction [28, 29]. As shown in Figure 3b, *β*-lapachone (yellow-colored compound) was similarly present in both top (PEG-rich) and bottom (dextran-rich) phase of dextran/4-arm PEG ATPS. In contrast, intense yellow color was visible from the top phase of dextran/4-arm PEG-*β*CD ATPS, suggesting that 4-arm PEG-*β*CD apparently had a stronger affinity for *β*-lapachone than 4-arm PEG.

The above finding was further corroborated by the partition coefficient measurements (Figure 3c). The partition coefficient of *β*-lapachone was near 1 in dextran/4-arm PEG ATPS, indicative of its equal distribution in the top and bottom phases. However, the partition coefficient of *β*-lapachone was significantly ($^{***}P < 0.001$) increased to ~4.3 in dextran/4-arm PEG-*β*CD ATPS. This phenomenon was likely caused by the formation of a strong host-guest pair between *β*CD and *β*-lapachone with a high association constant (K_c = 1230 M^{-1}) [30]. It has been reported that *β*CD and *β*-lapachone can form 1:1 inclusion complexes through hydrophobic binding of the dimethyl moiety of *β*-lapachone within the apolar cavity of *β*CD (Figure S2) [31]. A similar trend was observed from imiquimod, but the effect of 4-arm PEG-*β*CD on its partition was weaker than the case of *β*-lapachone. For instance, 4-arm PEG-*β*CD induced 4.2-fold and 2.1-fold enhancement in the partition coefficient of *β*-lapachone and imiquimod, respectively, compared to 4-arm PEG. The relatively low association constant (K_c = 23.3 M^{-1}) of *β*CD-imiquimod inclusion complex was probably responsible for the smaller enhancement in the partition coefficient of imiquimod [32]. On the other hand, 4-arm PEG-*β*CD had a minimal impact on the partition behavior of oxaliplatin, which was preferentially distributed in the dextran-rich phase as evidenced by its partition coefficient < 1. These results demonstrated the ability of 4-arm PEG-*β*CD to modulate the partitioning behavior of *β*-lapachone and imiquimod in ATPS.

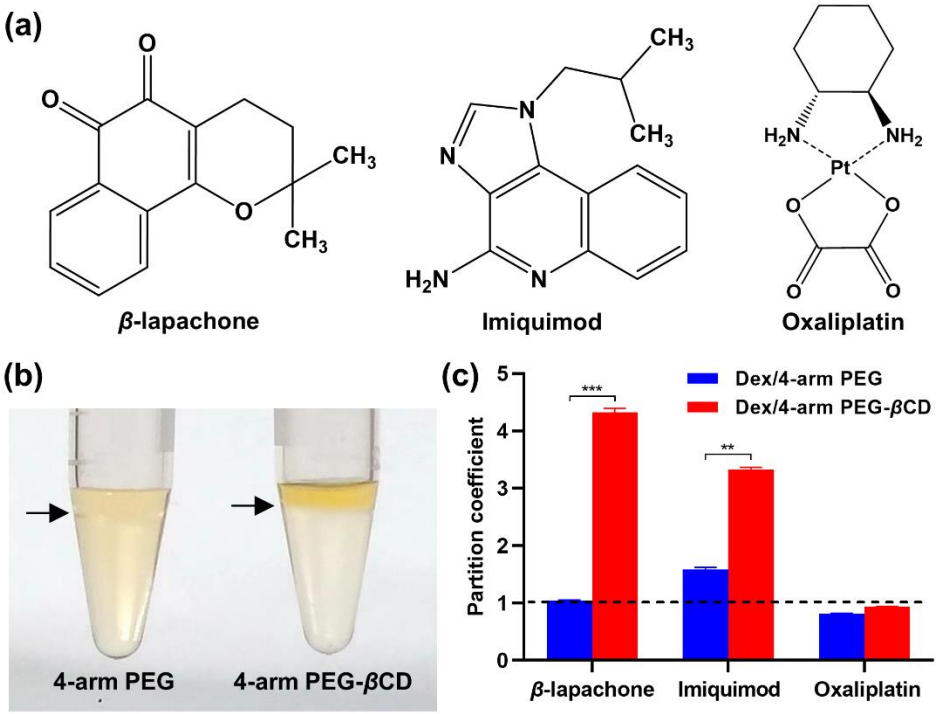

Figure 3. (a) Chemical structure of the small-molecule drugs tested in this study. (b) Photograph showing the partitioning of *β*-lapachone (yellow-colored compound) in two-phase mixtures composed of dextran/4-arm PEG (left) or dextran/4-arm PEG-*β*CD (right). The arrows indicate the interface between the PEG-rich top and dextran-rich bottom phase. (c) Partition coefficients of *β*-lapachone, imiquimod and oxaliplatin in the different two-phase mixtures. The dashed line indicates the partition coefficient of 1. Mean ± SD (n = 3); $^{**}P < 0.01$; $^{***}P < 0.001$.

3.3. Formation and characterizaion of Dex-Tyr/4-arm PEG-βCD hydrogels

The formation of Dex-Tyr/4-arm PEG-*β*CD hydrogels was accomplished by adding diluted H_2O_2 and HRP into a single-phase mixture of Dex-Tyr conjugate, 4-arm PEG-*β*CD and drug of interest. HRP was selected as a gelation catalyst because of its ability to induce fast gelation (within a few minutes) without the need for additional co-factors [28]. As depicted in Figure 4a, the storage modulus (G') began to increase upon addition of H_2O_2 and HRP, and then exceeded loss modulus (G'') gradually, implying that crosslinking of Dex-Tyr conjugates occurred as a result of HRP-catalyzed coupling of phenol groups [16]. The gel point at which sol-to-gel transition occurs was determined as 1.5 ± 0.2 min, indicating the rapid formation of a crosslinked gel network. The resultant Dex-Tyr/4-arm PEG-*β*CD hydrogel appeared opaque presumably due to the scattering of visible light by the phase-separated structure [15]. To elucidate the phase-separated structure inside the hydrogel, we used red-fluorescent PEG-sulforhodamine and green-fluorescent FITC-dextran to stain the PEG-rich and dextran-rich phase, respectively. Confocal laser scanning microscopy confirmed the existence of spherical 4-arm PEG-*β*CD domains with an average diameter of

2.4±0.8 μm (Figure 4b). As observed in the bright field image, the micrometer-sized domains were present in a high density within the hydrogel, which could be beneficial for increasing the likelihood of capturing drug molecules via the host-guest complexation.

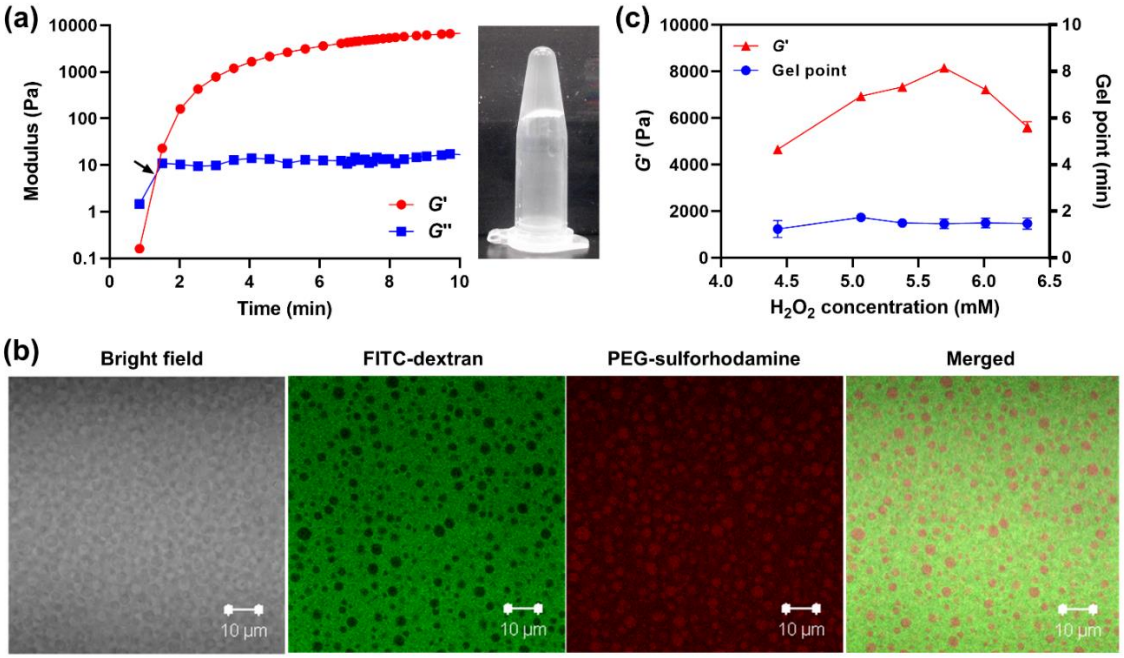

Figure 4. (a) Time-course change of storage modulus (G') and loss modulus (G'') for Dex-Tyr/4-arm PEG-βCD hydrogel. The arrow indicates the gel point. The resultant hydrogel appears opaque due to presence of microdomains (inset). (b) Confocal microscopy images of Dex-Tyr/4-arm PEG-βCD hydrogel labeled with FITC-dextran (green) and PEG-sulforhodamine (red). Scale bar = 10 μm. (c) G' and gel point of Dex-Tyr/4-arm PEG-βCD hydrogels produced at various H_2O_2 concentrations. HRP concentration was fixed to 0.13 units mL^{-1}. Mean ± SD (n = 3).

Figure 4c shows the change in G' and gel point of Dex-Tyr/4-arm PEG-βCD hydrogels at varying H_2O_2 concentrations. When H_2O_2 concentration was raised from 4.43 to 5.69 mM, G' value of the hydrogels gradually increased from 4.65 to 8.16 kPa, indicating the increased formation of Tyr-Tyr crosslinks at higher concentrations of H_2O_2 [20]. However, a further increase in H_2O_2 concentration resulted in a drastic drop of G', possibly owing to the inactivation of HRP associated with the destruction of its heme structure by phenoxyl radicals [33]. On the other hand, the gel point remained almost constant in the range of 1.5-1.6 min regardless of H_2O_2 concentration, suggesting that the mechanical strength of Dex-Tyr/4-arm PEG-βCD hydrogels could be tuned solely by the amount of H_2O_2 without impacting the gelation speed. It has been reported that the G' value of hydrogels typically increases with their crosslink density and thus influences on the diffusivity of entrapped drugs across the gel network [34]. Hence, for fair comparison of drug release kinetics, we formulated all tested hydrogels with identical G' by adjusting the amount of H_2O_2 added. Dex-Tyr and Dex-Tyr/4-

arm PEG-*β*CD hydrogels having the same *G′* of ~7.3 kPa were produced using 5.38 mM H_2O_2, whilst 6.65 mM H_2O_2 were employed to prepare Dex-Tyr/4-arm PEG hydrogels with the identical *G′* (Figure S3).

To further understand the mechanical properties of the produced hydrogels, we assessed the effect of shear strain and angular frequency on *G′* and *G″*' values. As shown in Figure 5a, the dynamic strain sweep test revealed that *G′* of Dex-Tyr/4-arm PEG-*β*CD hydrogel was independent of the applied shear stress, indicative of its stable network structure [35]. It was also found that the hydrogel exhibited a solid-like rheological behavior (*G′* >> *G″*'). In the dynamic frequency sweep test (Figure 5b), *G′* of Dex-Tyr/4-arm PEG-*β*CD hydrogel remained constant over a broad frequency range of 0.1−100 rad/s, suggesting that the gel network structure was maintained entirely by covalent bonds [36]. Notably, there was little difference in the strain/frequency sweep profiles between Dex-Tyr/4-arm PEG-*β*CD and Dex-Tyr/4-arm PEG hydrogels. This finding demonstrated that the introduction of *β*CD did not significantly affect the viscoelasticity and mechanical stability of Dex-Tyr/4-arm PEG hydrogels.

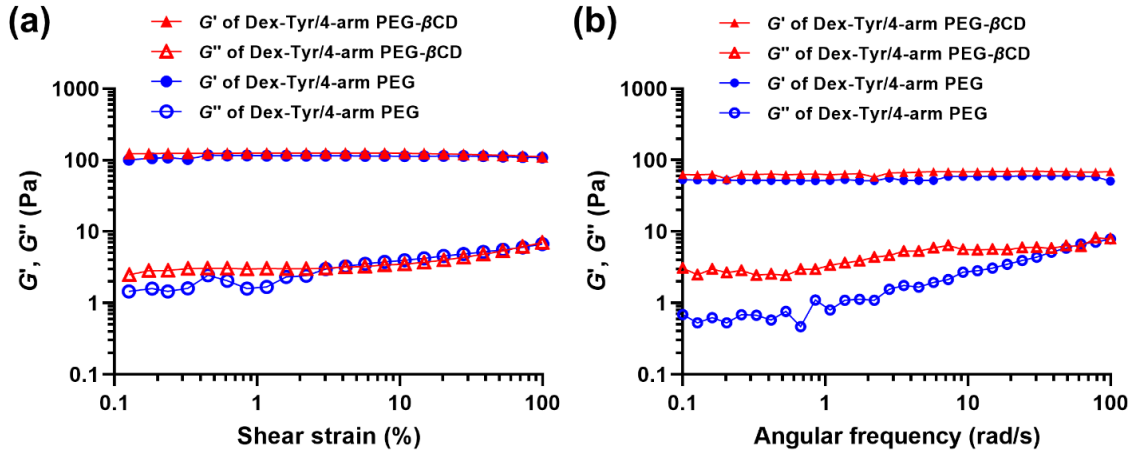

Figure 5. (a) Dynamic strain sweep measurement of Dex-Tyr/4-arm PEG-*β*CD and Dex-Tyr/4-arm PEG hydrogels with angular frequency at 10 rad/s. (b) Dynamic frequency sweep measurement of the hydrogels with strain at 1%.

3.4. Assessment of drug release kinetics

We investigated the release profile of *β*-lapachone from Dex-Tyr, Dex-Tyr/4-arm PEG and Dex-Tyr/4-arm PEG-*β*CD hydrogels with identical storage moduli in PBS solution (pH 7.4) at 37 ºC (Figure 6a). As expected, an initial burst effect was detected for Dex-Tyr hydrogels. For example, nearly 90% of *β*-lapachone was liberated from Dex-Tyr hydrogels within 22 h, probably due to the free diffusion of the drug molecules across the gel network [37]. Interestingly, there was only a marginal difference in the drug release pattern between Dex-Tyr and Dex-Tyr/4-arm PEG hydrogels, whereas Dex-Tyr/4-arm PEG-*β*CD hydrogels exhibited a sustained release of *β*-lapachone for a longer period of time (~93% over 192 h).

This finding implies that the host-guest complexation between *β*CD and *β*-lapachone might play a crucial role in suppressing the initial burst effect. During the release period, Dex-Tyr/4-arm PEG-*β*CD hydrogels became slightly swollen (~1.7-fold increase in normalized gel weight) but still appeared opaque, suggesting the microdomains remained stable in the physiological environment (Figure S4). To check the integrity of *β*-lapachone liberated from Dex-Tyr/4-arm PEG-*β*CD hydrogels, its inherent fluorescence was examined in the release fraction taken at 192 h [30]. Notably, the release fraction showed a similar fluorescence emission spectrum to that of the native *β*-lapachone, suggesting that no denaturation of *β*-lapachone occurred during the encapsulation and release process (Figure 6b).

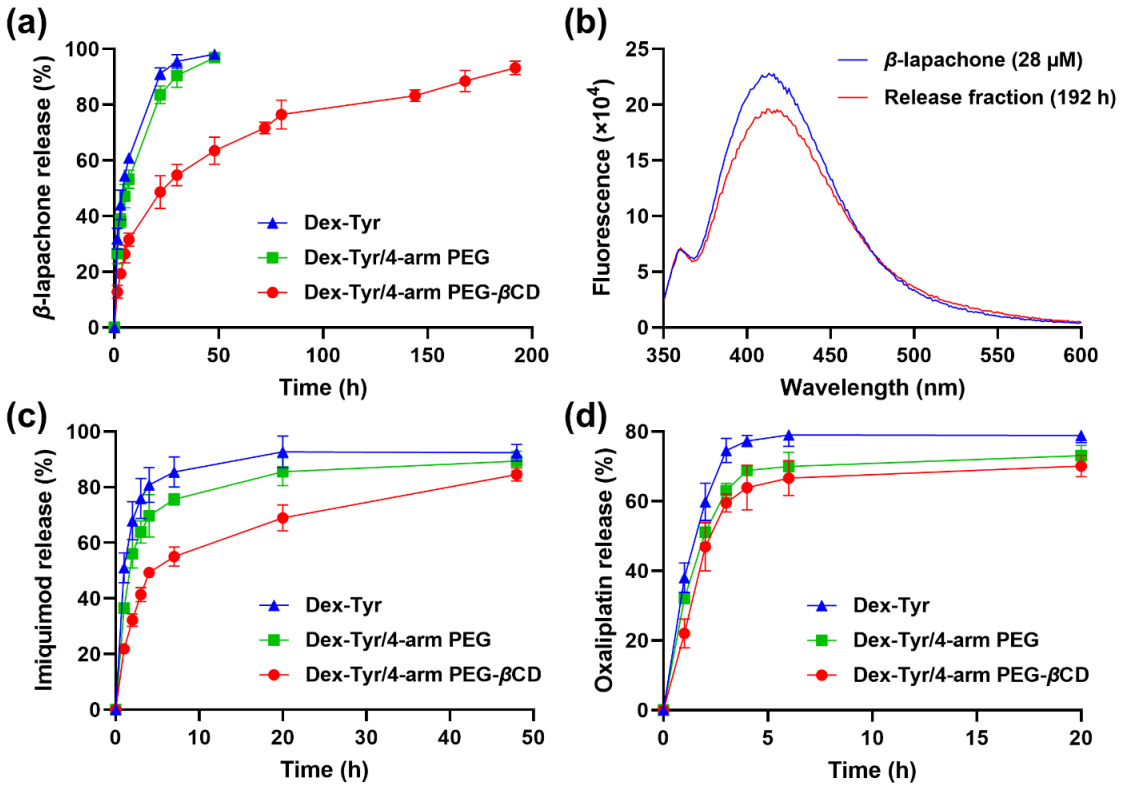

Figure 6. (a) Cumulative release of *β*-lapachone from Dex-Tyr, Dex-Tyr/4-arm PEG or Dex-Tyr/4-arm PEG-*β*CD hydrogels. (b) Comparison of fluorescence emission spectra (λ_{ex}=320 nm) between *β*-lapachone (28 μM) and the release fraction taken at 192 h. (c,d) Cumulative release of (c) imiquimod and (d) oxaliplatin from Dex-Tyr, Dex-Tyr/4-arm PEG or Dex-Tyr/4-arm PEG-*β*CD hydrogels. Mean ± SD (*n* = 3).

As shown in Figure 6c, imiquimod was rapidly diffused out from both Dex-Tyr and Dex-Tyr/4-arm PEG hydrogels. Unlike *β*-lapachone, the release of imiquimod was only slightly delayed in Dex-Tyr/4-arm PEG-*β*CD hydrogel. For instance, about 32% of *β*-lapachone was liberated from Dex-Tyr/4-arm PEG-*β*CD hydrogel for 7 h, whilst over 55% of imiquimod was released from the hydrogel during the same period. Considering that the host-guest pair between *β*CD and imiquimod had much lower association constant (K_c = 23.3

M^{-1}) [32] than the one between *β*CD and *β*-lapachone (K_c = 1230 M^{-1}) [30], the less sustained release of imiquimod was probably attributed to the formation of a weaker inclusion complex between the drug and 4-arm PEG-*β*CD. In the case of oxaliplatin, there was negligible difference in the drug release kinetics among all three hydrogels (Figure 6d). Thus, it was conceivable that 4-arm PEG-*β*CD had little impact on the diffusional release of oxaliplatin, presumably due to its preferred distribution in dextran-rich phase as observed in Figure 3c.

To analyze the drug release mechanism, we calculated the diffusional exponent (*n*) of the tested hydrogel formulations using the Ritger-Peppas equation [22]. As presented in Table 1, all the experimental release data were well fitted to the Ritger-Peppas equation with relatively high correlation coefficients (R^2 > 0.93). The *n* values for both Dex-Tyr and Dex-Tyr/4-arm PEG hydrogels were close to 0.5 regardless of the drug payload, revealing that Fickian diffusion was the dominant mechanism in the transport of small-molecule drugs from these hydrogels. It was also found that the release of oxaliplatin from Dex-Tyr/4-arm PEG-*β*CD hydrogel was governed by Fickian diffusion. On the other hand, Dex-Tyr/4-arm PEG-*β*CD hydrogel exhibited the *n* value of 0.597 and 0.614 for the release kinetics of *β*-lapachone and imiquimod, respectively, suggesting that these drugs were liberated from the hydrogel by anomalous non-Fickian diffusion mechanism. This phenomenon was likely ascribed to the prevention of drug diffusion from the gel matrix via the formation of an inclusion complex in discrete 4-arm PEG-*β*CD microdomains. Collectively, the above results demonstrated that the phase-separated hydrogels can be potentially applied for prolonged release of small-molecule drugs via host-guest complexation.

Table 1. Analysis of drug release kinetics

Hydrogel	Drug	*n* [a]	R^2	Release mechanism
Dex-Tyr	*β*-lapachone	0.482 ± 0.017	0.991 ± 0.009	Fickian diffusion
Dex-Tyr/4-arm PEG	*β*-lapachone	0.505 ± 0.025	0.997 ± 0.003	Fickian diffusion
Dex-Tyr/4-arm PEG-*β*CD	*β*-lapachone	0.597 ± 0.006	0.999 ± 0.001	Non-Fickian diffusion
Dex-Tyr	Imiquimod	0.489 ± 0.010	0.970 ± 0.018	Fickian diffusion
Dex-Tyr/4-arm PEG	Imiquimod	0.519 ± 0.022	0.979 ± 0.014	Fickian diffusion
Dex-Tyr/4-arm PEG-*β*CD	Imiquimod	0.614 ± 0.020	0.937 ± 0.018	Non-Fickian diffusion
Dex-Tyr	Oxaliplatin	0.503 ± 0.023	0.967 ± 0.053	Fickian diffusion
Dex-Tyr/4-arm PEG	Oxaliplatin	0.519 ± 0.064	0.931 ± 0.027	Fickian diffusion
Dex-Tyr/4-arm PEG-*β*CD	Oxaliplatin	0.521 ± 0.065	0.979 ± 0.021	Fickian diffusion

[a] The correlation coefficient (R^2), diffusional exponent (*n*), and drug release mechanism were determined using the Ritger-Peppas equation. The mean and SD values from triplicates (*n* = 3) are presented here.

4. Conclusion

In this study, novel phase-separated hydrogels with 4-arm PEG-*β*CD microdomains were developed for controlled release of small-molecule drugs. Dextran/4-arm PEG-*β*CD ATPS exhibited significantly larger partition coefficients of *β*-lapachone and imiquimod compared to dextran/4-arm PEG ATPS. The formation of Dex-Tyr/4-arm PEG-*β*CD hydrogel was accomplished by HRP/H_2O_2-mediated enzymatic crosslinking reaction. The presence of spherical PEG-rich microdomains inside the hydrogel was confirmed by confocal laser scanning microscopy. The phase-separated hydrogel was found to liberate nearly 93% of the incorporated *β*-lapachone over 192 h in a sustained manner. Release kinetics analysis revealed that the transport of *β*-lapachone and imiquimod across the gel network took place by non-Fickian diffusion mechanism. Our study may propose a potential strategy to modulate the drug release kinetics of polymeric hydrogels for various biomedical applications.

Acknowledgments

This work was supported by the Institute of Bioengineering and Bioimaging (Biomedical Research Council, Agency for Science, Technology and Research (A*STAR)), Singapore.

Conflicts of Interests

The authors declare no conflict of interest.

Authors' contribution

Conceptualization, K.H.B. and M.K.; investigation, K.H.B., S.N. and L.L.; data curation, K.H.B. L.L.; writing—original draft preparation, K.H.B.; writing—review and editing, K.H.B. and S.N.; funding acquisition, M.K; supervision, M.K.

References

[1] Peters JT, Wechsler ME, Peppas NA. Advanced Biomedical Hydrogels: Molecular Architecture and Its Impact on Medical Applications. *Regen. Biomater.* 2021, 8(6): 1–21.

[2] Wu C, Liu J, Zhai Z, Yang L, Tang X, Zhao L, Xu K, Zhong W. Double-Crosslinked Nanocomposite Hydrogels for Temporal Control of Drug Dosing in Combination Therapy. *Acta Biomater.* 2020(106): 278–288.

[3] Cho IS, Ooya T. Cell-Encapsulating Hydrogel Puzzle: Polyrotaxane-Based Self-Healing Hydrogels. *Chem. – A Eur. J.* 2020, 26(4): 913–920.

[4] Park SG, Li MX, Cho WK, Joung YK, Huh KM. Thermosensitive Gallic Acid-Conjugated Hexanoyl Glycol Chitosan as a Novel Wound Healing Biomaterial. *Carbohydr. Polym.* 2021(260): 117808.

[5] Burdick JA, Mauck RL, Gerecht S. To Serve and Protect: Hydrogels to Improve Stem Cell-Based Therapies. *Cell Stem Cell* 2016, 18(1): 13–15.

[6] Foster AA, Marquardt LM, Heilshorn SC. The Diverse Roles of Hydrogel Mechanics in Injectable Stem Cell Transplantation. *Curr. Opin. Chem. Eng.* 2017(15): 15–23.

[7] Swartzlander MD, Barnes CA, Blakney AK, Kaar JL, Kyriakides TR, Bryant SJ. Linking the Foreign Body Response and Protein Adsorption to PEG-Based Hydrogels Using Proteomics. *Biomaterials* 2015(41): 26–36.
[8] Ngo BKD, Grunlan MA. Protein Resistant Polymeric Biomaterials. *ACS Macro Lett.* 2017, 6(9): 992–1000.
[9] Vermonden T, Censi R, Hennink WE. Hydrogels for Protein Delivery. *Chem. Rev.* 2012, 112(5): 2853–2888.
[10] Li J, Mooney DJ. Designing Hydrogels for Controlled Drug Delivery. *Nat. Rev. Mater.* 2016, 1(12): 16071.
[11] Huang X, Brazel CS. On the Importance and Mechanisms of Burst Release in Matrix-Controlled Drug Delivery Systems. *J. Control. Release* 2001, 73(2–3): 121–136.
[12] Din Fud, Kim DW, Choi JY, Thapa RK, Mustapha O, Kim DS, Oh Y-K, Ku SK, Youn YS, Oh KT, Yong CS, Kim JO, Choi HG. Irinotecan-Loaded Double-Reversible Thermogel with Improved Antitumor Efficacy without Initial Burst Effect and Toxicity for Intramuscular Administration. *Acta Biomater.* 2017(54): 239–248.
[13] Iqbal M, Tao Y, Xie S, Zhu Y, Chen D, Wang X, Huang L, Peng D, Sattar A, Shabbir MAB, Hussain HI, Ahmed S, Yuan Z. Aqueous Two-Phase System (ATPS): An Overview and Advances in Its Applications. *Biol. Proced. Online* 2016, 18(1): 18.
[14] Chao Y, Shum HC. Emerging Aqueous Two-Phase Systems: From Fundamentals of Interfaces to Biomedical Applications. *Chem. Soc. Rev.* 2020, 49(1): 114–142.
[15] Moriyama K, Yui N. Regulated Insulin Release from Biodegradable Dextran Hydrogels Containing Poly (Ethylene Glycol). *J. Control. Release* 1996, 42(3): 237–248.
[16] Bae KH, Lee F, Xu K, Keng CT, Tan SY, Tan YJ, Chen Q, Kurisawa M. Microstructured Dextran Hydrogels for Burst-Free Sustained Release of PEGylated Protein Drugs. *Biomaterials* 2015, 63, 146–157.
[17] Bae KH, Kurisawa M. Emerging Hydrogel Designs for Controlled Protein Delivery. *Biomater. Sci.* 2016, 4(8): 1184–1192.
[18] Yamamoto K, Ooya T. Modulation of Protein Partition in an Aqueous Two Phase System by Inclusion Complexation of Cyclodextrins. *Chem. Lett.* 2019, 48(12): 1551–1554.
[19] Sun G, Mao JJ. Engineering Dextran-Based Scaffolds for Drug Delivery and Tissue Repair. *Nanomedicine* 2012, 7(11): 1771–1784.
[20] Lee F, Bae KH, Kurisawa M. Injectable Hydrogel Systems Crosslinked by Horseradish Peroxidase. *Biomed. Mater.* 2015, 11(1): 14101.
[21] Bae KH, Tan S, Yamashita A, Ang WX, Gao SJ, Wang S, Chung JE, Kurisawa M. Hyaluronic Acid-Green Tea Catechin Micellar Nanocomplexes: Fail-Safe Cisplatin Nanomedicine for the Treatment of Ovarian Cancer without off-Target Toxicity. *Biomaterials* 2017(148): 41–53.
[22] Peppas N. Hydrogels in Pharmaceutical Formulations. *Eur. J. Pharm. Biopharm.* 2000, 50(1): 27–46.
[23] Tripodo G, Wischke C, Neffe AT, Lendlein A. Efficient Synthesis of Pure Monotosylated Beta-Cyclodextrin and Its Dimers. *Carbohydr. Res.* 2013(381): 59–63.
[24] Yu H, Feng Z, Zhang A, Sun L, Qian L. Synthesis and Characterization of Three-Dimensional Crosslinked Networks Based on Self-Assemly of α-Cyclodextrins with Thiolated 4-Arm PEG Using a Three-Step Oxidation. *Soft Matter* 2006, 2(4): 343.
[25] Fu SC, Chau YP, Lu KS, Kung HN. β-Lapachone Accelerates the Recovery of Burn-Wound Skin. *Histol. Histopathol.* 2011, 26(7): 905–914.
[26] Lee J, Chuang TH, Redecke V, She L, Pitha PM, Carson DA, Raz E, Cottam HB. Molecular Basis for the Immunostimulatory Activity of Guanine Nucleoside Analogs:

Activation of Toll-like Receptor 7. *Proc. Natl. Acad. Sci.* 2003, 100(11): 6646–6651.

[27] Tesniere A, Schlemmer F, Boige V, Kepp O, Martins I, Ghiringhelli F, Aymeric L, Michaud M, Apetoh L, Barault L, Mendiboure J, Pignon JP, Jooste V, van Endert P, Ducreux M, Zitvogel L, Piard F, Kroemer G. Immunogenic Death of Colon Cancer Cells Treated with Oxaliplatin. *Oncogene* 2010, 29(4): 482–491.

[28] Moreira Teixeira LS, Feijen J, van Blitterswijk CA, Dijkstra PJ, Karperien M. Enzyme-Catalyzed Crosslinkable Hydrogels: Emerging Strategies for Tissue Engineering. *Biomaterials* 2012, 33(5): 1281–1290.

[29] Bae JW, Choi JH, Lee Y, Park KD. Horseradish Peroxidase-Catalysed in Situ - Forming Hydrogels for Tissue-Engineering Applications. *J. Tissue Eng. Regen. Med.* 2015, 9(11): 1225–1232.

[30] Nasongkla N, Wiedmann AF, Bruening A, Beman M, Ray D, Bornmann WG, Boothman DA, Gao J. Enhancement of Solubility and Bioavailability of Beta-Lapachone Using Cyclodextrin Inclusion Complexes. *Pharm. Res.* 2003, 20(10): 1626–1633.

[31] Wang F, Blanco E, Ai H, Boothman DA, Gao J. Modulating B-lapachone Release from Polymer Millirods through Cyclodextrin Complexation. *J. Pharm. Sci.* 2006, 95(10): 2309–2319.

[32] Ramineni SK, Cunningham LL, Dziubla TD, Puleo DA. Development of Imiquimod-Loaded Mucoadhesive Films for Oral Dysplasia. *J. Pharm. Sci.* 2013, 102(2): 593–603.

[33] Schmidt A, Schumacher JT, Reichelt J, Hecht HJ, Bilitewski U. Mechanistic and Molecular Investigations on Stabilization of Horseradish Peroxidase C. *Anal. Chem.* 2002, 74(13): 3037–3045.

[34] Bae KH, Wang LS, Kurisawa M. Injectable Biodegradable Hydrogels: Progress and Challenges. *J. Mater. Chem. B* 2013, 1(40): 5371.

[35] Lee F, Chung JE, Kurisawa M. An Injectable Enzymatically Crosslinked Hyaluronic Acid–Tyramine Hydrogel System with Independent Tuning of Mechanical Strength and Gelation Rate. *Soft Matter* 2008, 4(4): 880.

[36] Sathaye S, Mbi A, Sonmez C, Chen Y, Blair DL, Schneider JP, Pochan DJ. Rheology of Peptide- and Protein-Based Physical Hydrogels: Are Everyday Measurements Just Scratching the Surface? *Wiley Interdiscip. Rev. Nanomedicine Nanobiotechnology* 2015, 7(1): 34–68.

[37] Axpe E, Chan D, Offeddu GS, Chang Y, Merida D, Hernandez HL, Appel EA. A Multiscale Model for Solute Diffusion in Hydrogels. *Macromolecules* 2019, 52(18): 6889–6897.